Chapter

Distributed, Advanced Fiber Optic Sensors

Sanjay Kher and Manoj Kumar Saxena

Abstract

India is poised to use nuclear energy in a big way. The safety of these systems depends upon monitoring various parameters in hazardous environment like high radiation, high temperature exceeding 1000°C, and gas/coolant leakages. In this chapter, we shall dwell on basics of distributed sensing, related instrumentation, device fabrication, and actual advanced field applications. Techniques like Raman scattering, resonance response of fiber gratings, and selective absorption are employed for design, development, and fabrication of distributed sensors and devices. Raman distributed sensors with advanced data processing techniques are finding increasing applications for fire detection, coolant leak detection, and safety of large structures. The systematic investigations related to portable systems developed at the author's lab have been described. Wavelength-encoded fiber gratings are the attractive candidate for high gamma radiation dose measurements in environment such as particle accelerators, fission reactors, food processing facilities, and ITER-like installations. The basics of fiber gratings, their operational designs, and devices based on fiber gratings have been described with advanced applications like high temperature sensing, strain measurements at cryogenic temperatures, and strain in nuclear environment. Finally, novel approaches are described for distributed hazardous gas monitoring for large areas such as airports, train stations, and reactor containment buildings.

Keywords: Raman optical fiber distributed temperature sensor, fiber Bragg grating sensor, long period grating sensor, dynamic self-calibration, strain sensors for nuclear environment

1. Introduction

The discovery of lasers in the 1960s and development of low loss silica optical fiber opened a new era of fiber optic sensors. Intrinsic insensitivity to electromagnetic interference (EMI), remote detection, operational ability in hazardous environment, and potential for distributed sensing make them especially useful for monitoring large nuclear infrastructures such as coolant monitoring, reactor containment buildings, nuclear waste storage sites etc. [1–5]. Radiation tolerant fibers can be used in various configurations for distributed sensing of temperature, strain, and several other parameters avoiding the requirement of positioning many discreet sensors [6–11]. Further, the radiation sensitive fibers can be used for radiation dose monitoring for local dose deposition measurements, hot spot dose monitoring in waste storage facilities, surveillance at airports and ports of entry, etc. With the

availability of lasers, fibers, and low noise detectors in the mid-IR region, it has become possible to design novel distributed sensor devices for sensing hazardous volatile compounds for homeland security especially at airports, underground metro stations, and big event areas.

A wide range of techniques such as intensity modulation, wavelength encoding, and polarization provide powerful sensing capabilities. Further, several detection techniques have been investigated for development of optical fiber-based distributed sensors. Radiation-induced absorption, scintillation, fluorescence, optically stimulated luminescence, and induced refractive index changes have been used for real-time dose measurements. Optical fiber grating [12–15]-based specialty sensors have been used for distributed strain measurements in very low temperature, very high temperature, or high radiation environment. Raman and Brillouin scattering-based techniques are used for distributed temperature measurements for fire and hot spot detection. Mid-IR and near-IR absorption measurements coupled with hollow core fibers are used for leak detection of hazardous gases. This chapter will describe the basic principles, main components, various sensing systems for advanced applications, and future potential of distributed fiber sensors.

2. What is distributed sensing?

Distributed sensing is a technique whereby one sensor cable is capable to collect data (continuous/quasi-continuous profiling) that are spatially distributed over many individual measurement points. The various modes of sensing can be understood from **Figure 1** [3, 4]. Briefly, a point sensor means monitoring a parameter at a discreet point; a quasi-distributed sensor system involves an arrangement of a finite number of discreet sensors as a linear array, while in fully distributed sensing mode, the measuring parameter of interest is monitored continuously along the fiber path, providing a spatial mapping of the parameter along fiber.

In conventional sensing, say for temperature, an individual sensor such as a thermocouple or platinum probe is needed for each point of interest whereas distributed sensing addresses many points simultaneously along with their spatial location [5]. With proper design architecture, it can contribute to enhanced safety and security by providing early warnings of gas and coolant leakages, structural cracks, onset of fire, hot spot detection in pipelines, radiation leaks, etc. Two techniques such as optical time-domain reflectometry (OTDR) [4, 16–23] and

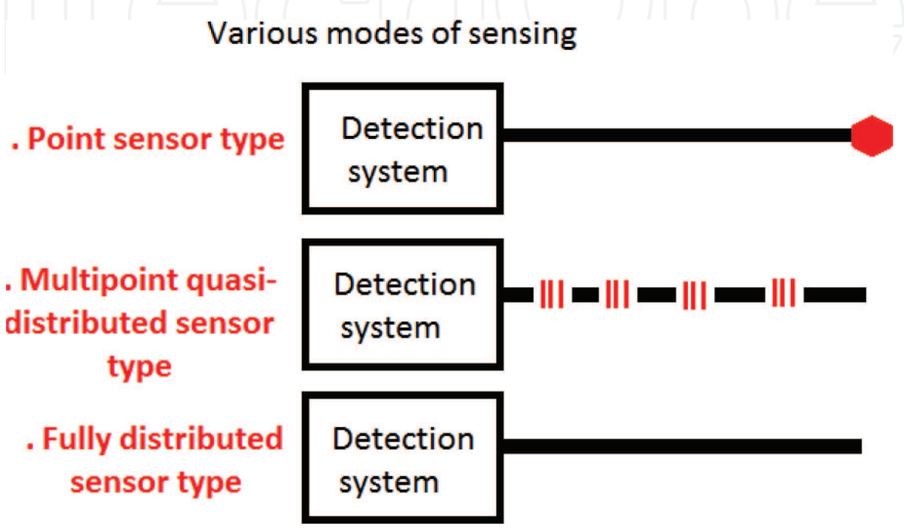

Figure 1.
Various modes of sensing: point, multipoint quasi-distributed, and fully distributed.

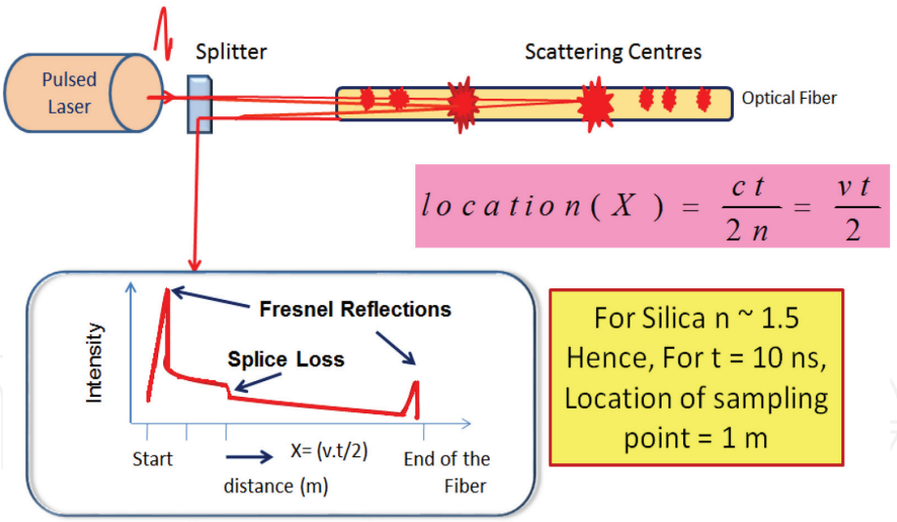

Figure 2.
Schematic diagram of OTDR.

wavelength division multiplexing (WDM) are generally used for distributed sensing. In OTDR (**Figure 2**), a pulsed laser is coupled to an optical fiber through a directional coupler/splitter. The backscattered light originating from density and composition variation is monitored continuously in time. The spatial location of an event is determined from time of flight measurements, that is, the device calculates the distance of the measuring point based on the time it takes for the reflected light to return.

For example, if the backscattered light is detected after 10 ns from the starting point, it is set to originate from 1 m distance from origin of fiber. This can be easily calculated from OTDR equation $X = ct/2n$, where X is the distance from origin (start of fiber taken as zero time), t is the time of event detection, c (3×10^8 m/s) is the velocity of light in the vacuum, and n is the refractive index of fiber for wavelength of operation. If we use a sensing fiber with core refractive index (n) of 1.5 and wish to measure distance (X) traveled after t = 10 ns, then it is easy to calculate that X = 1.0 m by putting the values in OTDR equation [21, 23].

In wavelength multiplexing, a device such as Bragg grating is used to encode a series of resonant wavelengths in the fibers [12–15]. The wavelengths in turn are monitored by wavelength interrogator. The resonant wavelengths are affected by measuring parameters and are thus monitored in a quasi-distributed manner.

3. All fiber Raman optical fiber distributed temperature sensor with dynamic self-calibration

Temperature sensors are ubiquitous devices that permeate our daily lives. Many areas of temperature measurements require a large area of coverage with high localization accuracy. Raman optical fiber-based distributed temperature sensors (ROFDTSs) are equipped with the ability of providing temperature values as a continuous function of distance along the fiber. In an ROFDTS, every bit of fiber works as a sensing element as well as data transmitting medium, to substitute the role played by several point sensors, thus allowing reduced sensor network cost. ROFDTSs have attracted the attention as a means of temperature monitoring and fire detection in power cables, long pipelines, bore holes, tunnels, and critical installations like oil wells, refineries, induction furnaces, and process control industries. The basic principle of temperature measurement using ROFDTS involves

Raman scattering [10] in conjunction with OTDR. The ratio of Raman anti-Stokes (AS) and Stokes (St) intensities is used for determination of unknown temperature. The AS signal is strongly dependent on temperature, while the Stokes signal is slightly dependent on temperature. Based on time of flight and intensity of Stokes and anti-Stokes signals, location and temperature information can be retrieved. The backscattered light has many spectral components as shown in **Figure 3** [24]. For temperature measurements, Raman components are analyzed.

The OTDR principle allows estimation of the location of hot zone whereas Raman scattering permits measurement of temperature of the hot zone. Sensing fiber is coupled to short interrogating laser pulses, and backscattered AS and St components are monitored for signal changes. Unknown temperature of hot zones can be estimated from the ratio (R) of AS and St using the following expression [11]

$$R = \frac{I_{as}}{I_s} = \left(\frac{\lambda_s}{\lambda_{as}}\right)^4 \exp\left(-\frac{hc\nabla}{kT}\right) \tag{1}$$

where λ_s and λ_{as} are the Stokes and anti-Stokes optical signal wavelengths, ∇ is their wave number separation from the pump laser wavelength, h is Planck's constant, c is the velocity of light, and k is Boltzmann's constant. AS is the main signal which carries the signature of temperature variation whereas St provides reference and eliminates a number of effects common to both the signals. One can simplify Eq. (1) by replacing known terms by B where,

$$B = \frac{hc\nabla}{k} \tag{2}$$

Since values of h, c, and k are known, the numerical value of B is found to be 631.3 for silica fiber having ∇ = 440 cm^{-1}.

One can simplify the profile analysis by referencing the ratio profile at unknown temperature to the ratio value at known temperature of a pre-selected calibration zone of fiber. The temperature of a given zone T (°C) is then given by the following expression [25].

$$T(^{\circ}\mathrm{C}) = B.\left[\frac{1}{\left(B.\frac{1}{\theta} - \ln R_T + \ln R_\theta\right)}\right] - 273 \tag{3}$$

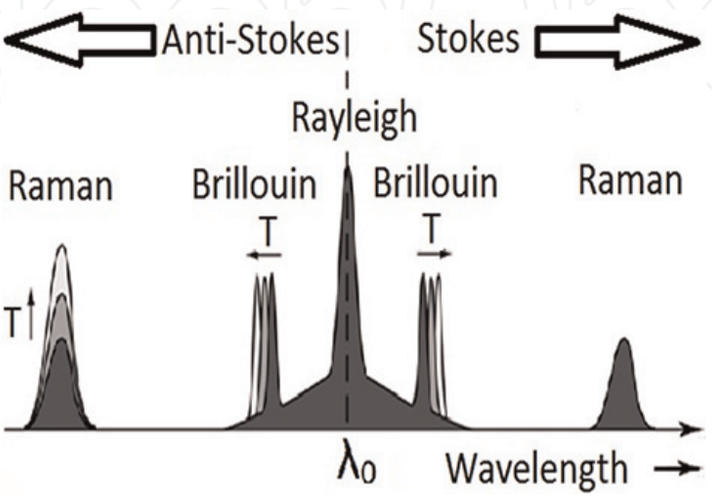

Figure 3.
Backscattered laser light from optical fiber in the case of Raman and Brillouin scattering (source: https://www.google.co.in/search?q=BACKSCATTERED+LASER+LIGHT&source=lnms&tbm=isch&sa=X&ved=0ahUKEwiCvf-iq9jcAhWKT30KHdJ4CjYQ_AUICigB&biw=1093&bih=530) (images) [24].

Here, the calibration zone is kept at some known absolute room temperature (Θ). Eq. (3) can be deduced after taking the quotient of the ratio profile at unknown temperature (R_T) for an arbitrary zone and the ratio value at the calibration zone (R_Θ) and solving it for T. Parameter (R_Θ) is the ratio value of AS to St signal (AS/St) for the calibration zone (at temperature Θ) of length 1 m chosen from sensing fiber at the laser end. In Eq. (3), parameters B and Θ are known. Therefore, Eq. (3) will yield temperature profile (T in °C) for complete fiber length, provided that profiles of R_T and value of R_θ are available.

Figure 4 shows the block diagram of Raman optical fiber distributed temperature sensor.

Further, **Figure 5** gives an idea of averaged anti-Stokes Raman signal for a 2.5 m long zone heated by a proportional intergral derivative (PID) controlled heating oven.

To determine the unknown temperature profile with certain accuracy for complete fiber length by using Eq. (1), appropriate measures are to be devised and implemented to address several error-causing issues. These issues are described as below [21, 23]. The author's laboratory has successfully solved these issues and designed a field portable unit.

3.1 Issue no. 1

The first issue is the difference in theoretical and experimental values of the ratio (R) at various temperature values. For example, at room temperature (25°C, say), the theoretical and experimental values of R are 0.1693 and 0.55, respectively. At 50°C, the theoretical and experimental values of R are found to be 0.1995 and 0.658, respectively. On the other hand, the theoretical and experimental values are 0.2415 and 0.8279, respectively, at 85°C. The reason for this difference is explained below [23].

At 25°C (for example), obtaining a theoretical value of 0.1693 for R requires that the optoelectronic conversion using photomultiplier tube (e.g. PMT-R5108, Hamamatsu) detectors, the beam splitting, and the subsequent light coupling into AS and St detectors are in such a way that the relation St = 5.906 × AS is maintained for backscattered AS and St signals while traveling the path from fiber to the final stage of detection. However, due to nonideal behavior of various optical components in

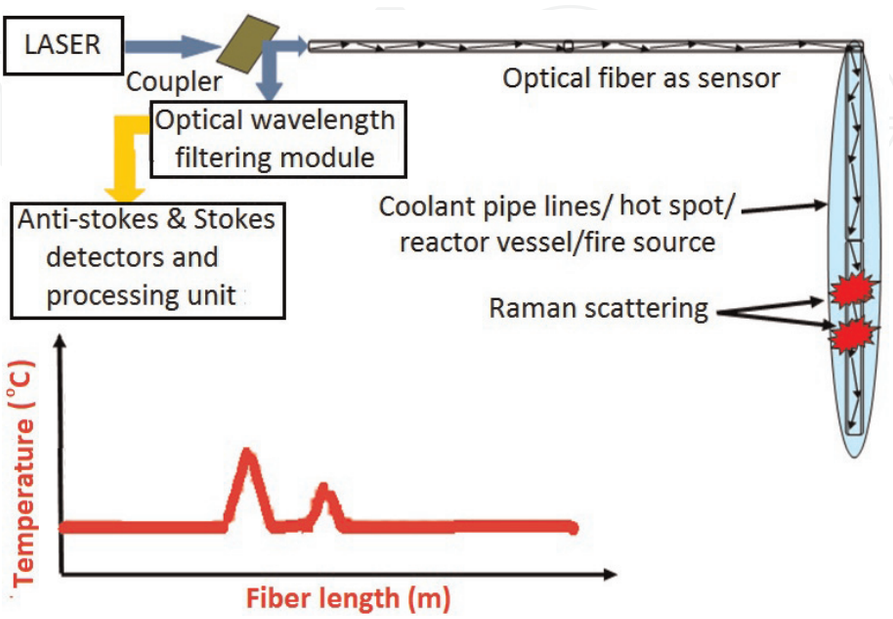

Figure 4.
Block diagram of Raman optical fiber distributed temperature sensor.

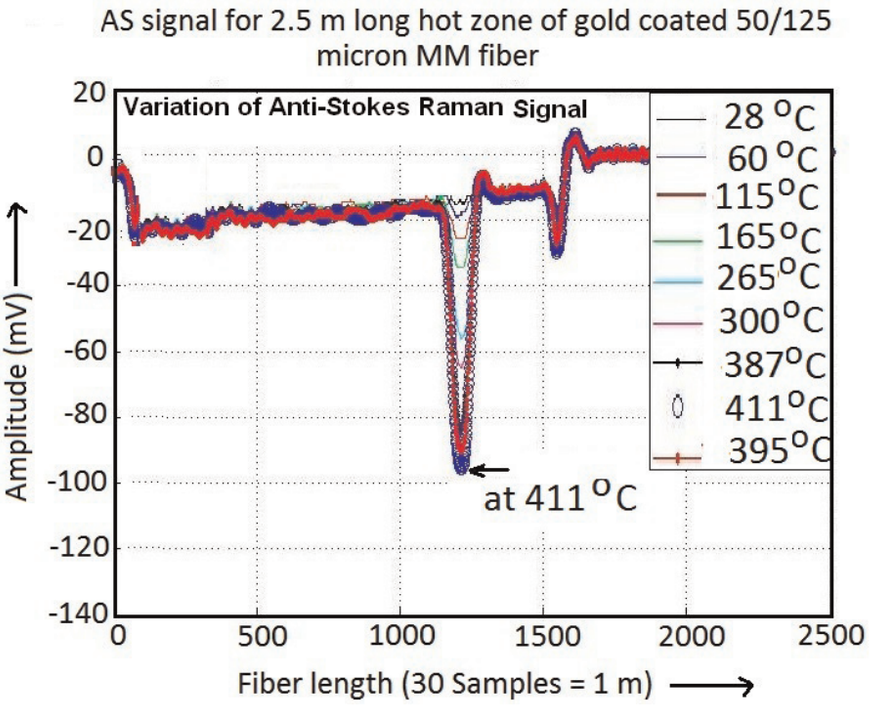

Figure 5.
The anti-Stokes Raman signal profile at various temperatures.

the path and band nature of AS and St signals, the above relation does not hold. The relation gets deteriorated at every stage in the path. For example, the cathode radiant sensitivity of a PMT for AS wavelength (1018 nm) and St wavelength (1109 nm) is 0.95 mA/W and 0.2mA/W, respectively, which causes St current to be approximately 5 times less compared to AS current. Nonideal performance of beam splitters and optical filters also does not support the above ideal relation. As a result, the cumulative effect of various components makes experimental values of R to be different from the theoretical one.

Direct use of experimental values of R in Eq. (1) will yield highly erroneous and unacceptable temperature profile (T). Hence, Eq. (1) needs to be modified to obtain correct values. Modification is done by referencing the experimentally obtained ratio values with respect to the ratio value at some known temperature of calibration zone which is chosen from sensing fiber itself.

3.2 Issue no. 2

The second issue is the nonidentical fiber attenuation along the fiber length for Raman AS and St signals due to difference in their wavelengths [9, 11]. In a typical system using 1064 nm excitation laser, the difference between two wavelengths is ~90 nm. The lower optical wavelength signal (AS) experiences higher attenuation in comparison to higher optical wavelength signal (St) while traveling in sensing optical fiber. This attenuation difference results in an unwanted downward slope in ratio (R) profile and finally in unknown temperature (T) profile with respect to fiber length. It may be noted that downward slope in ratio (R) profile causes additional errors in unknown temperature (T) profile of fiber and should be corrected.

3.3 Issue no. 3

While de-noising Raman AS and St signals for better signal-to-noise ratio (SNR), conventional finite impulse response/infinite impulse response (FIR/IIR)-based

Fourier filtering causes spatial inaccuracy in locating the hot-zones which in turn yields erroneous information about the location of hot zones [18].

3.4 Issue no. 4

The amplitude of AS and St signals varies with time due to slow variations/drifts in laser power and laser-fiber coupling. Also, the temperature of calibration zone itself may change unless it is controlled by a dedicated setup. Therefore, any previously stored reference values of AS and St signals and calibration zone temperature can no longer be used as a reference for temperature measurement at a later stage.

3.5 Approaches to solve the problematic issues

Stoddart et al. [20] proposed to use Rayleigh instead of St from the backscattered spectrum to avoid the temperature measurement error in hydrogen-rich environments due to differential attenuation caused by the optical fiber for AS and St signal wavelengths. This resulted in better results but could not eliminate the error caused by the differential attenuation completely. The dual-ended (DE) configuration [26] (i.e. both ends of sensing fiber are connected to ROFDTS unit) and dual laser source schemes [27, 28] have also been proposed to take care of the difference in attenuation between AS and St. These schemes have resulted in improvements but add complexity and need double length of fiber, extra distributed temperature sensor (DTS) with an optical switch, and two costly lasers. A correction method to take care of the difference in attenuation for AS and St signals has been proposed with only one light source and one light detector but requires attachment of a carefully designed reflective mirror at the far fiber-end of the sensing fiber [29]. Recently, a more sophisticated correction technique [30] based on detection of AS signal alone in combination with DE configuration has been investigated. ROFDTSs based on the above schemes are important and to a certain extent become mandatory in situations where sensing fiber is exposed to the severe radiation environment or hydrogen darkening in oil wells. Requirements for less demanding situations like temperature measurement in steam pipelines of turbines, electrical cables and temperature profiling of big buildings, gas pipelines and mines etc. can be met by the technique based on digital signal processing.

In order to address the above issues satisfactorily, a discrete wavelet transform (DWT)-based dynamic self-calibration and de-noising technique is used and implemented by the authors as given in detail [23]. Briefly, wavelets are mathematical functions that can be used to segregate data into various frequency components. Each component can then be studied with a resolution matched to its scale. In DWT, a signal may be represented by its low frequency component and its high frequency component.

The DWT-based technique is simpler, more automatic, and provides a single solution to address all the above issues simultaneously. The DWT technique takes care of the difference in optical attenuation for AS and St signals by using their trend and also de-noises the AS and St signals while preserving spatial locations of peaks. Also, this technique requires just 1 m long calibration zone which is much less than the 100 m required in the previous technique. Moreover, the dynamic measurement of calibration zone's temperature eliminates the requirement of keeping the calibration zone at a constant temperature, and thus, complicated heating arrangement is avoided. Actual wavelet transform-based processed signal profile is shown in **Figure 6**. **Table 1** presents the comparison of error in temperature measurement at various zones using Eq. (3) with unprocessed and processed Raman signals. Both absolute errors and percentage errors (in brackets) are

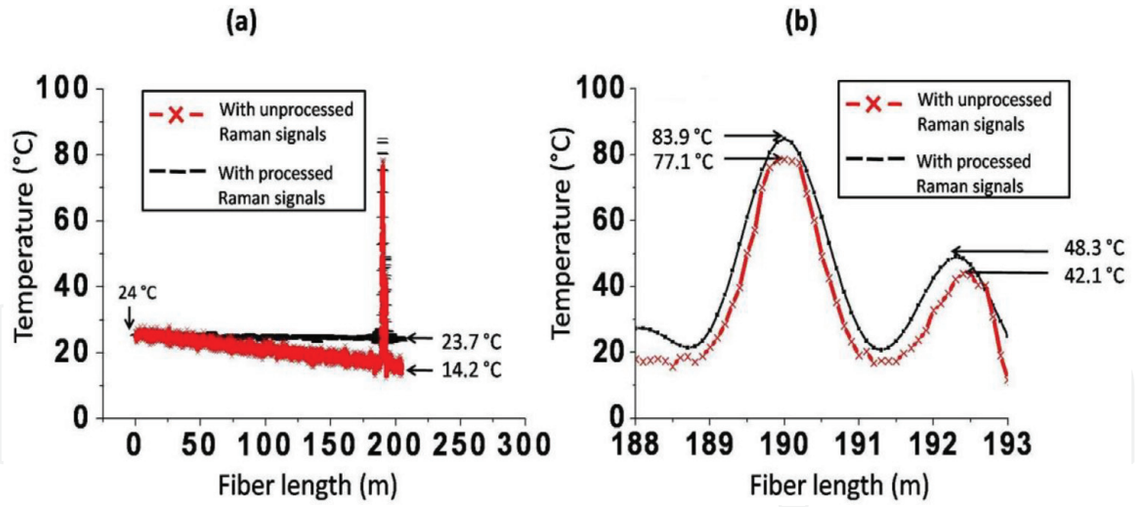

Figure 6.
Distributed temperature profile with processed (black color) and unprocessed (red color) Raman signals: (a) view for complete fiber length and (b) zoomed view for hot zones.

Zone (location)	Reference temperature	Measured temperature	
		Unprocessed	Processed
Start of fiber (location: 0 m)	24.5°C	24°C	24°C
	Error	−0.5°C (−2.04%)	−0.5°C (−2.04%)
Hot zone-1 (location: 190 m)	85°C	77.1°C	83.9 °C
	Error	−7.9 °C (−9.29%)	−1.1 °C (−1.29%)
Hot zone-2 (location: 192.4 m)	50°C	42.1°C	48.3°C
	Error	−7.9°C (−15.8%)	−2.4°C (−3.4%)
End of fiber (location: 205 m)	25°C	14.2 °C	23.7°C
	Error	−10.8°C (−43.2%)	−1.3°C (−5.2%)

Table 1.
Comparison of error in temperature measurement at various zones with unprocessed and processed Raman signals.

reported to appreciate the improvement achieved after processing of Raman signals.

Fiber Sensors Lab., Raja Ramanna Centre for Advanced Technology (RRCAT), Indore, India has developed a Raman scattering-based OFDTS [23] with the following specifications, and the developed OFDTS is capable of working in high accelerating voltage (1.5 MV), magnetic field (1.5 T), and bremsstrahlung radiation present in accelerator systems.

(a) Temperature range: 25–300°C, (b) temperature resolution: 3°C, (c) spatial resolution: 1 m (over a length of 500 m); can be improved to few cm with special fiber-laying techniques, (d) distance (dynamic range for distance covered): 500 m, (e) fire alarm: audio-visual alarms can be generated, and (f) gamma field operation; can operate up to a gamma dose of 1 MGy.

For more ruggedness and field deployability, an all-fiber ROFDTS scheme is desirable. The schematic design of one such scheme is depicted in **Figure 7**. Recently, a distributed sensor using a superconducting nanowire single photon detector and chalcogenide fiber has been proposed. This scheme has the potential to

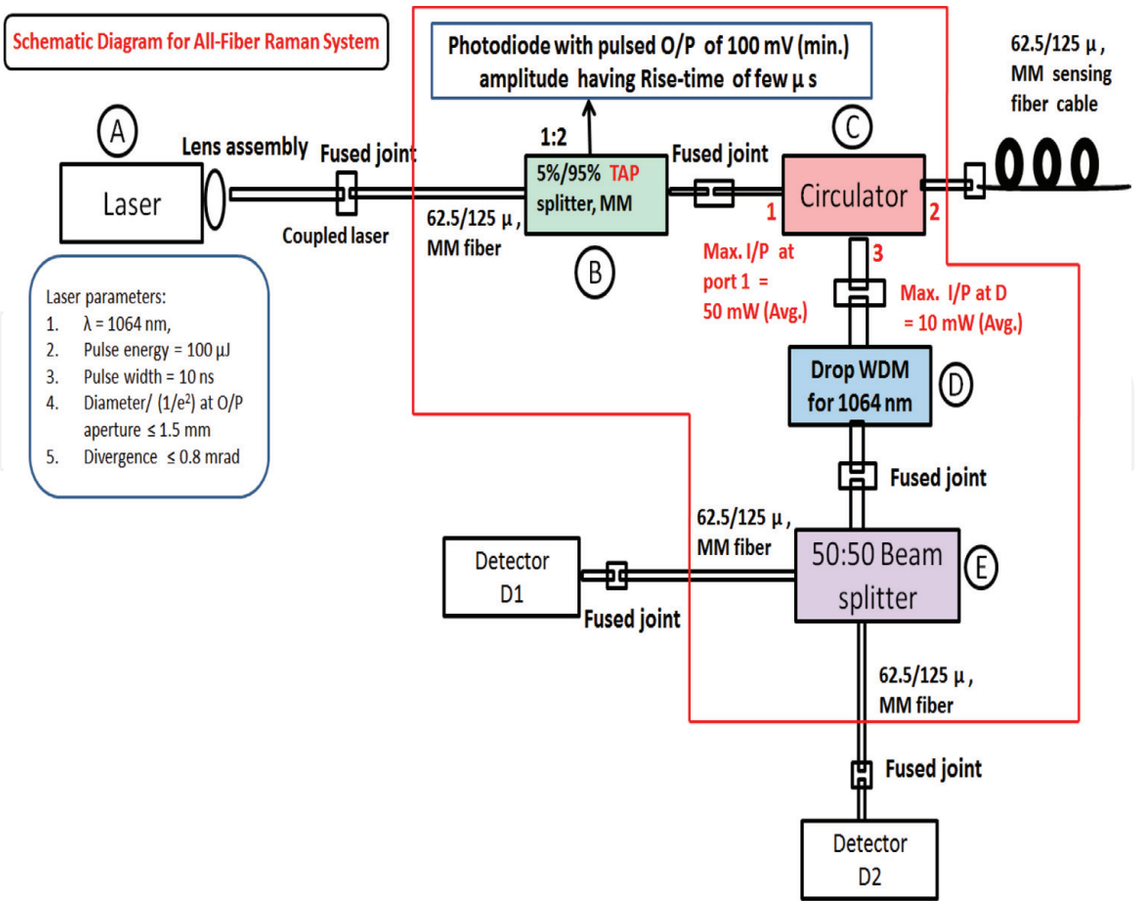

Figure 7.
Schematic diagram of an all-fiber-based ROFDTS scheme.

offer sub-centimeter spatial resolution sensor, below 1°C temperature resolution over a distance of few hundreds of meters.

4. Quasi-distributed sensors for temperature and strain measurements

The fiber Bragg gratings (FBG) were first written by Hill et al. [12] who discovered the breakthrough phenomena of photosensitivity in optical fiber. As a result of this development, FBG-based strain and temperature sensors came into existence. The method of writing FBG in sensing fiber's section involves creation of periodic modulation of fiber core's refractive index. The refractive index is modulated by spatial pattern of ultraviolet (UV) light between 240 and 260 nm. The periodic structure in fiber's core can be created by phase mask method [13, 15]. A particular pattern in a particular segment of fiber will correspond to a specific Bragg reflection wavelength. The multiple gratings can be fabricated by using a specific phase mask with different initial Bragg wavelength gratings in the same fiber causing creation of several point sensors in a single sensing fiber. Such FBG-based sensors are quasi-distributed temperature sensors where temperature sensing by fiber is possible only where grating was created.

According to Bragg's law, when a broad band light is injected into the optical fiber consisting of FBG sensors, a specific wavelength of light is reflected by FBG [15]. The Bragg wavelength is determined by the product of effective refractive

index (n_{eff}) of the grating and the grating period (Λ) (also called pitch length) as given by the following equation:

$$\lambda_B = 2n_{eff}\Lambda \tag{4}$$

Figure 8 depicts the basic principle of FBG reflection spectra and interrogation technique [12–15]. The Bragg wavelength depends on grating period of FBG and the refractive property of optical fiber.

It is clear from Eq. (4) that any change in the pitch length or refractive index will induce a shift in the resonant wavelength. Consequently, temperature, strain or deformations of the fiber can be monitored by the corresponding resonant wavelength shift. The Bragg wavelength is strain- and temperature-dependent through physical elongation or thermal change of the sensor and through the change in the fiber refractive index due to photoelastic and thermo-optic effects.

There are essentially three types of gratings which vary in photosensitivity. They are known as type I, II, and IIA with the details of each type given in [15]. Type I gratings are written with moderate intensities and exhibit an index grating right across the core. Type II gratings can be written with much higher intensities within very short times, often with a single nanosecond pulse from an excimer laser (single shot damage gratings). Type IIA gratings are regenerated gratings (RGs) specifically designed for high temperature operation. In addition, there are different physical types of gratings such as long period gratings (LPGs), chirped gratings, tilted (blazed) gratings, and micro-structured FBGs. Typical temperature sensitivity of FBG is 10 pm/°C (at 1550 nm in standard silica-based single mode fiber) and strain sensitivity is 1.2 pm/micro-strain [13].

A strong point of FBGs is their capability of multiplexing in wavelength that enable multiple points or quasi-distributed sensing. The schematic diagram of the distributed FBG sensor is shown in **Figure 9**.

There have been significant developments in two of the areas that have constrained the progress of fiber grating technology. Firstly, the issue of temperature and strain isolation has been overcome by using various techniques reported in the literature, from simply having collocated sensors that are exposed to the same temperature fluctuations to isolate stress and strain, to more complex methods, such as using tilted or chirped gratings to distinguish between the different measurands. Secondly, with improved data processing methods, simpler interrogation techniques are being utilized such that the optical signal can easily be transposed into the electrical domain, allowing the optical networks to be interfaced seamlessly with electronic systems. In addition, the production of FBGs has improved significantly through draw tower processes and automated manufacturing. One of the main advantages of FBG sensors is their ability to be easily

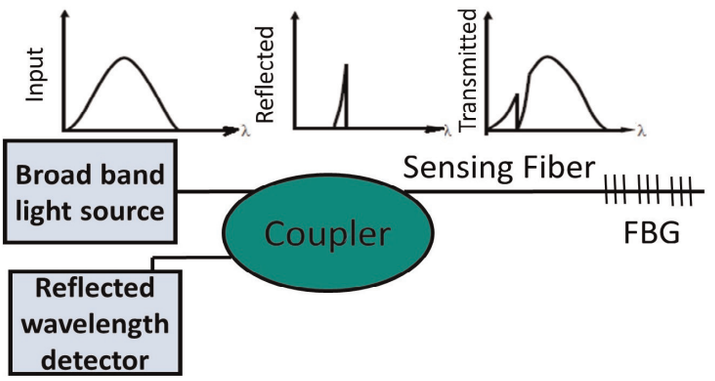

Figure 8.
Schematic representation of FBG sensor.

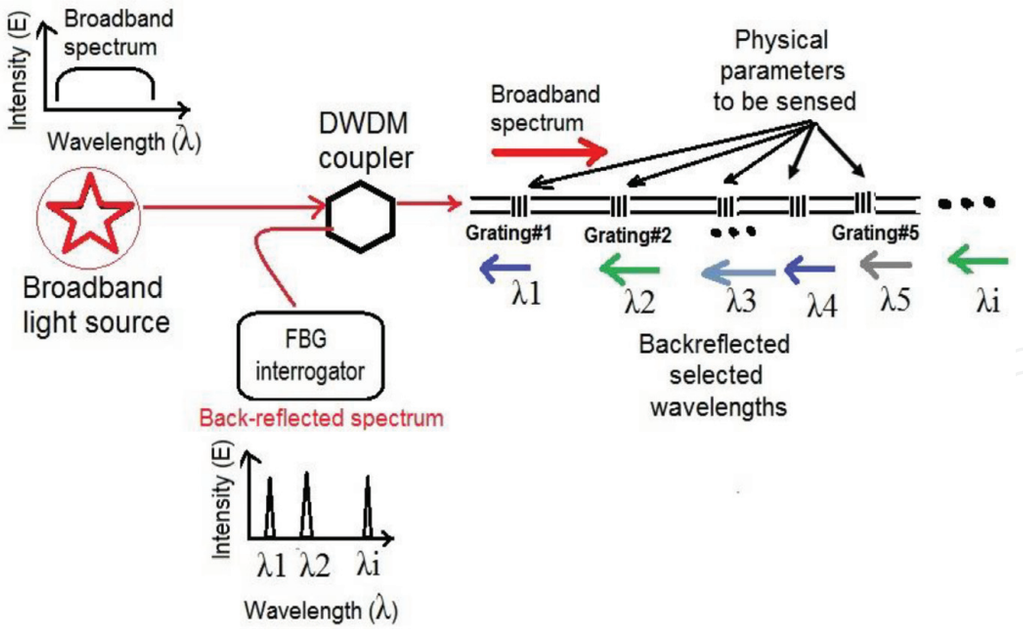

Figure 9.
Schematic diagram of the distributed FBG sensor.

multiplexed through time division multiplexing (TDM) and wavelength division multiplexing (WDM). The information from each sensor must be separated and interpreted, which requires an interrogator system to interrogate many FBGs connected in series.

A series of wavelength-encoded FBGs are used for quasi-distributed sensing applications. Several groups developed quasi-distributed FBG sensors for temperature and strain monitoring [31–33]. Central Glass & Ceramic Research Institute (CGCRI), Kolkata, India recently developed specially packaged FBGs for strain/force monitoring of electric railway engine pantographs. However, very special packaging or specialty fibers were required for advanced applications such as strain monitoring at high temperature, strain monitoring at cryogenic temperature, and very high temperature monitoring exceeding 1000°C. FBG strain sensor for health monitoring of structure at 600°C have also been developed.

5. Ultra-high temperature distributed sensors

The dynamic range of ROFDTS is restricted by coating on the optical fiber. Polyimide coatings can permit measurement up to 350°C while the gold coating may allow the measurement up to 600°C. Beyond this, distributed sensing is possible by specialized gratings made in specialized fibers. For ultra-high temperature sensing, type II-IR gratings in silica optical fiber withstand a temperature of up to 1000°C, which are usually fabricated by using a femto-second laser with power density near the damage threshold of the fiber glass. These gratings however have disadvantages as sensing elements because of asymmetric reflection spectrum and a large spectral width of more than 0.6 nm. These create problems during distributed sensing. Gratings written on a different host material, namely sapphire gratings, can be used as a temperature-sensing probe up to 1900°C. However, the material and mode mismatch with normal silica-based optical fiber and high cost of fabrication restricts its use in distributed sensing. Identification of structural changes on a molecular scale involved with the formation of a new type of FBG named

regenerated Bragg grating based on annealing a conventional Type-I FBG to create a new, more robust one seems to be a promising candidate to achieve better sustainability at high temperature. However, in standard photosensitive silica fiber, RG gratings were found to be stable only below 950°C.

CGCRI, Kolkata, India in collaboration with RRCAT, Indore, India has taken up the development of a new glass composition-based photosensitive fiber to fabricate RG for temperature ~1400°C. The fiber is likely to be based on yttrium-stabilized zirconia-calcium-alumina-phospho silica glass. The motivation of the choice of such kind of multi-material glass-based optical fiber is to increase the photosensitivity along with thermal stability of fabricated RG. The regeneration takes place near the fiber glass transition temperature, in which the transformation of the glass from monoclinic structure to tetragonal structure occurs. The ultra-high temperature sustainability of RG will be evaluated for the special composition through material study, which definitely is not achievable in a standard germano-silicate fiber. This work is expected to provide a new degree of freedom in the design of optical fiber sensor for ultra-high temperature sensing. This will open up opportunities in sectors such as power plants, turbines, combustion, and aerospace engineering where often the environments are too harsh for existing FBG sensor technology and will offer a new degree of freedom in the design of optical fiber sensors.

6. Strain sensors for nuclear environment

6.1 Wavelength encoded strain sensors

A long period fiber grating sensor in photonic crystal fiber with a strain sensitivity of −2.0 pm/με and negligible temperature sensitivity is fabricated by use of CO_2 laser beam. Such a strain sensor can effectively reduce the cross sensitivity between strain and temperature. Due to single material (pure silica) construction, they have been shown to be resistant to nuclear radiation and are thus useful for applications in secondary loops of nuclear reactors. The authors' lab has designed and developed such sensor devices.

6.2 Design principle

Photonic crystal fibers (PCFs) also known as holey fibers are a new class of optical fibers that have attracted intense scientific research during past few years. Typically, these fibers incorporate a number of air holes that run along the length of the fiber, and the size, shape, and distribution of the holes can be designed to achieve various novel wave-guiding properties that may not be possible in conventional fibers. Various PCFs have been demonstrated so far that exhibit remarkable properties such as endlessly single mode fiber, large mode area, and highly nonlinear performance. Temperature-insensitive long period gratings have attracted much attention because of their potential applications in achieving stable optical filters and gain flatteners as well as in realizing temperature-insensitive sensors for industrial and nuclear applications. Conventional fibers contain at least two different glasses, each with a different thermal expansion coefficient, thereby giving rise to high temperature sensitivity. PCFs are virtually insensitive to temperature because they are made of only one material (and air hole). This property can be used to obtain temperature-insensitive PCF-based devices. Long period gratings (LPGs) in PCF fibers have not yet been reported in India. Besides, the effect of high nuclear radiation on such PCF-based grating sensors has not been reported by any group to the best of our knowledge.

6.3 Theory

An LPG is formed by introducing periodic modulation of the refractive index along a single mode fiber. Such a grating induces light coupling from the fundamental guided mode to co-propagating cladding modes at discreet resonant wavelengths. LPGs in conventional fibers have been extensively used as band rejection filters, gain flattening filters, tunable couplers, and sensors. In general, as fiber devices and sensing elements, LPGs offer low back reflection, insensitivity to electromagnetic interference, and low insertion loss and cost effectiveness. For a long period grating with periodicity Λ, the wavelength $\lambda^{(m)}$ at which mode coupling occurs is given by

$$\lambda^{(m)} = \left(n_{eff} - n_{cl,m} \right) \Lambda \tag{5}$$

where n_{eff} is the effective refractive index of the propagating core mode at wavelength λ, and $n_{cl,m}$ is the effective refractive index of the mth cladding mode. The variation in the grating period and modal effective indices due to strain and temperature causes the coupling wavelength to shift. This spectral shift is distinct for each loss band and is a function of the order of corresponding cladding mode.

The axial strain sensitivity of LPGs may be examined by expanding Eq. (5) to yield

$$\frac{d\lambda}{d\varepsilon} = \frac{d\lambda}{d\left(\delta n_{eff}\right)} \left(\frac{dn_{eff}}{d\varepsilon} - \frac{dn_{cl}}{d\varepsilon} \right) + \Lambda \frac{d\lambda}{d\Lambda} \tag{6}$$

where $\delta_{neff} = (n_{eff} - n_{cl})$ is the differential effective index; ordinal m has been dropped for the sake of simplicity. The two terms on the right side can be divided into material (first term) and waveguide (second term) contributions. The temperature sensitivity of LPG grating is given by

$$\frac{d\lambda}{d\varepsilon} = \frac{d\lambda}{d\left(\delta n_{eff}\right)} \left(\frac{dn_{eff}}{dT} - \frac{dn_{cl}}{dT} \right) + \Lambda \frac{d\lambda}{d\Lambda} \frac{1}{L} \frac{dL}{dT} \tag{7}$$

where λ is the central wavelength of the attenuation band, T is the temperature, L is the length of the LPG, and Λ is the period of the LPG. For standard long period gratings with periodicity of hundreds of micrometers, the material effect dominates the waveguide contribution. Hence, only the first term in Eqs. (6) and (7) is considered for evaluation of sensitivity. For photonic crystal fibers which are single material fibers, the first term in Eq. (7) becomes negligible, resulting in very low temperature sensitivity. This term is an order smaller than that of B-Ge-doped photosensitive fiber. This opens-up the field for PCF-based temperature-insensitive sensors.

6.4 Device designs

Inscription of LPGs has been demonstrated using various techniques such as UV treatment, heat treatment with a CO_2 laser, or by applying mechanical pressure. Formation of LPG in pure-silica core PCF fibers is not straightforward because there is no photosensitivity provided by Ge-O_2 vacancy defect centers. The LPGs in PCF are primarily formed due to modification of glass structure. However, any geometrical deformation results in flaws or cracks that result in fracture of the fiber, and therefore, LPGs in PCF require high precision systems. Our fully automated CO_2 laser-based grating writing system can set the grating period in the range of

200–800 μm with a precision of 1 μm while laser intensity can be stabilized within ±5%. **Figure 10** shows the schematic diagram of our grating writing system. The fiber is exposed to CO_2 laser for a predetermined period and the beam is scanned repeatedly over the fiber until grating of sufficient strength is formed. This operation is performed through an AutoCAD program in which the period and length of the grating are selected as per the design requirement. This method is more accurate and free from vibration related uncertainties in the grating period. The spectral response is recorded using an optical spectrum analyzer (OSA) (86142B, Agilent) which is connected to LPG through patch-cords as shown in **Figure 10**.

During application of LPG-based strain sensors, one of the main difficulties is the cross sensitivity between strain and the temperature [34]. The common methods for cross sensitivity reduction are using temperature compensation and simultaneous strain and temperature measurement. Conventional fibers contain at least two different glasses, each with a different thermal expansion coefficient, thereby giving rise to high temperature sensitivity. By use of the CO_2 laser method, an LPG sensor with strain sensitivity of −0.45 pm/με and a temperature sensitivity of 59.0 pm/°C was written in corning SMF-28 fiber 2. Another LPG with a strain sensitivity of −0.19 pm/με and a temperature sensitivity of 10.9 pm/°C was described in PCF fiber. In this paper, we present a LPG-PCF sensor fabricated in ESM-PCF with a high strain sensitivity (−2.0 pm/με) and negligible temperature sensitivity.

For the preparation of LPFG in an endless-single-mode photonic crystal fiber (ESM-PCF), both ends of the PCF are fusion spliced to SMFs [34]. The loss for each splice is about 0.74 dB. An X-Y scanning CO_2 laser is used for the fabrication of LPGs in the ESM-PCF. The CO_2 laser operates at a frequency of 2 kHz and has a maximum power of 10 W. The laser power is controlled by the mark-speed of the laser pulses. The typical grating length and period in our experiment is 23.4 mm and 450 μm, respectively. **Figure 11** shows the transmission characteristics of a LPG fabricated on an ESM-PCF. Attenuation bands in the range of 1300–1700 nm have been investigated by an Optical spectrum analyzer.

The device has been tested on a standard strain calibration platform. **Figure 12** shows the strain-dependent wavelength shift of the fabricated device.

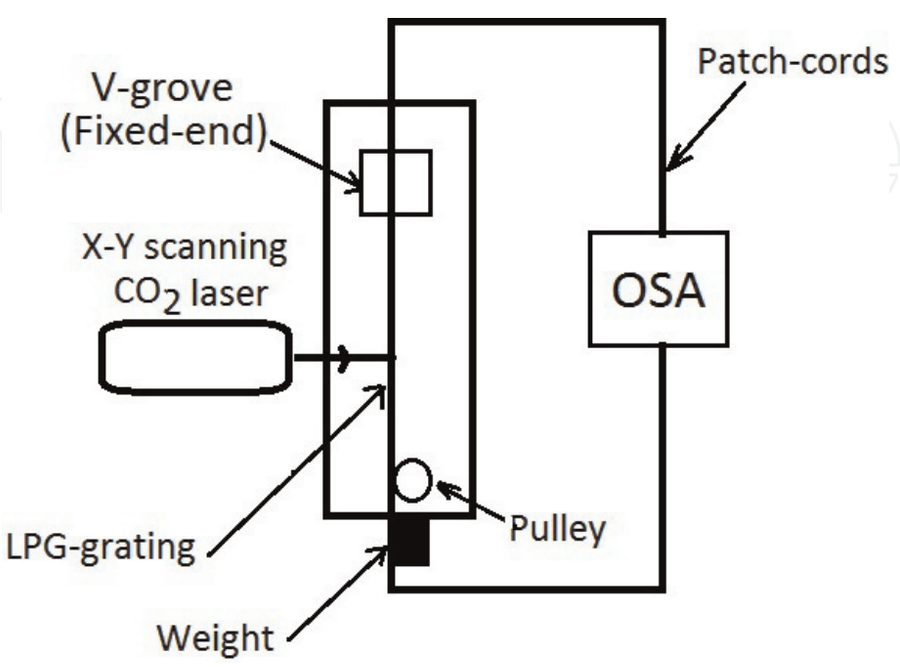

Figure 10.
Schematic diagram of long period grating fabrication set-up [34].

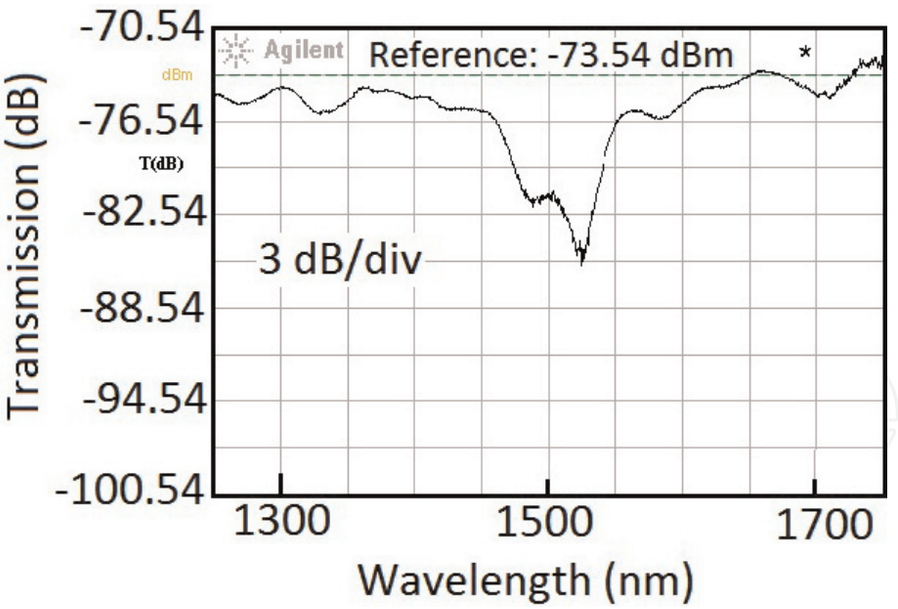

Figure 11.
Transmission characteristics of a LPG fabricated on an ESM-PCF with a period of 450 μm [34].

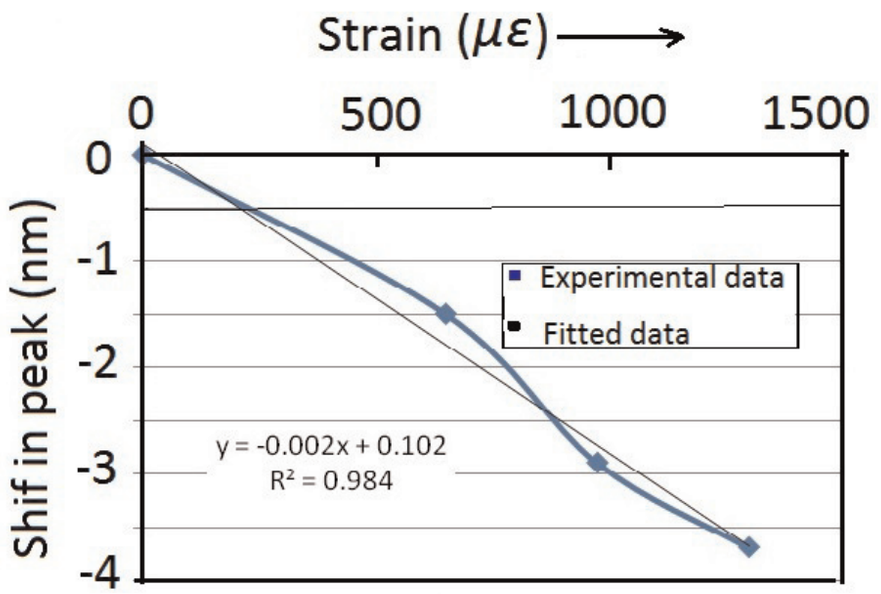

Figure 12.
Strain-dependent wavelength shift of LPG [34].

6.5 Strain sensors for cryogenic environment

The tendency of superconducting magnet coils to quench prematurely, at relatively low fractions of the critical current, or to exhibit training behavior, is often attributed to mechanical issues. Knowledge of stress, strain, and displacement of the windings is therefore central to the design of the superconducting magnet. The resistive foil strain gauge has remained the device most commonly used for measuring the strain on cryogenic structures. The nonlinear thermal apparent strains and measurement sensitivity to electromagnetic noise remain the most significant limitations to its successful implementation. FBG sensor has a number of distinct advantages over other sensors, such as EMI immunity, high sensitivity, and compact size. Furthermore, the wavelength-encoded nature allows the distributed sensing of strain. Fiber Bragg gratings are used to monitor temperature and strain in

engineering structures; to date, however, their use has been limited to ambient and high temperatures, typically in the range of 273–773 K.

There exist very few published reports on FBG strain sensors that have been functional at liquid nitrogen temperature. Zhang et al. have reported one such FBG sensor used to strain sensing at 77 K and used in high temperature superconducting magnet [29]. To date, an FBG sensor used to strain sensing at 4.2 K and used in low temperature superconducting magnet has not been reported. RRCAT, Indore is also working on FBG strain and temperature sensors for cryogenic applications. The sensors show linearity in strain range from 50 to 500 micro-strain at liquid nitrogen temperature.

6.5.1 Nuclear radiation sensors

Optical fibers offer a unique capability for remote monitoring of radiation in hazardous locations such as nuclear reactors and waste storage sites. Increase of attenuation, luminescence, and radiation-induced index change have been used to design dose sensors for dose ranges up to 100 kGy. The attenuation-based sensors based on specialty doped fibers reach a saturation level above 10 kGy. To overcome this limitation, alternative techniques such as changes in fiber gratings are explored. The wavelength-encoded operation of fiber gratings can solve many measurement problems such as radiation-induced broadband transmission loss in optical fibers, source fluctuation, etc. Most Bragg grating-based sensors, reported till date, are either less sensitive or reach a saturation level near 50–150 kGy depending on the composition and grating writing technique [29–33]. Recent publications have reported measurements only up to 100 kGy. The authors Henchel et al. [35] used specialty chiral gratings and reported measurements up to 100 kGy. However, the mode orders and fiber composition in sensitive gratings were not known. Rego et al. [36] have performed gamma dose measurements on arc-induced long period fiber gratings up to 500 kGy but found no measurable shift in the resonance wavelength. Gusarov et al. [16, 17, 37] have conducted high dose measurements on FBGs but did not find high sensitivity. We have discovered sensitive gratings in commercially available single mode fibers with known composition and mode orders [38, 39]. Our results and approach are described. These are believed to be the first studies of CO_2 written long period gratings up to 1 MGy.

6.5.2 Optical fiber composition optimization for high gamma dose and temperature sensing applications

Following requirements explain the need for novel radiation dose sensors:

a. Measurement of precise dose delivery is very crucial for treatment of cancer (40–50 Gy in about 20 sittings).

b. In the case of gamma source misplacement by universities or hospitals, it is important that state-of-the-art sensors away from the source are required.

c. Accelerators, fusion reactors, nuclear waste sites, and accidental leaks in reactors all require a sensitive, large area but remote dose sensors. Typically, the dose in various conditions and installations are: Tokamak Fusion reactor system, Japan (behind coils: 2 kGy, behind tiles: 200 MGy, 1.1 m behind port plug: 15 Gy). For space-based systems, total 10 year dose is around 100 kGy.

To cover a broad dose range from few Gy to 1 MGy, novel sensor systems like gratings are desirable. For most fibers, the increase in attenuation with dose saturates near few kGy which is accumulated within a relatively short time at certain critical locations and so they need to be replaced frequently. Even space-based systems are qualified for a dose up to 100 kGy.

6.5.3 Novel devices, fabrication technology, and testing for high radiation dose detection

Specialty doped fibers are required to measure high dose gamma radiation. These fibers should have negligible radiation-induced attenuation in IR but should show high index changes upon irradiation. Wavelength encoded fiber gratings are attractive candidates for high level gamma dose measurements in nuclear environment. This paper explains for the first time how arc-induced long period fiber gratings can be optimally designed for gamma dose measurements ranging from 1 kGy to 1 MGy.

We have investigated the gamma radiation effects on parameters of electric-arc-induced long period fiber gratings in high Ge doped and B/Ge co-doped single mode fibers. The grating resonance wavelength shifts and amplitude of the dips of various cladding modes were monitored on-line to study the role of grating fabrication and fiber chemical composition. These studies lead to identification of boron as a critical core dopant for high radiation sensitivity. After a Co-60 gamma dose of 1 MGy, the optimized gratings show radiation-induced changes of their transmission dip wavelength up to 20 nm which is comparable to CO_2 laser-induced gratings reported by us previously [39]. These gratings also show very high temperature sensitivity specially when operated in dispersion turn-around-point (TAP) mode [38].

Fibers doped with different boron contents in SiO_2-GeO_2-B_2O_3 host were fabricated indigenously under collaboration with CGCRI, Kolkata, India. The gratings in such fibers were modeled and analyzed. We have also designed and fabricated a stable and robust sensor package unit for remote gamma dose measurements up to a dose of 1 MGy. Lab trials of such units have been carried out, and the experience in using such devices for dose estimation is discussed. These devices make arc-induced LPGs and CO_2 laser-induced LPGs in Boron doped fibers a strong candidate for applications in super Large Hadron Collider (LHC) and International Thermonuclear Experimental Reactor (ITER). **Table 2** shows the experimental results of such online measurements.

Figure 13 shows our on-line gamma dose effect measurements using specialty turn-around-point (TAP) long period fiber grating.

Wavelength before exposure (nm)	Wavelength measured after 4.30 h of dose (dose of 3.6 kGy) after removal from gamma chamber (nm)
1161	1165.4
1229.6	1231
1250	1253.6
1364	1366.4
1546.7	No significant dip

Table 2.
Gamma radiation exposure data for LPG of a 400 micron grating period inscribed in Fiber Logix, SM G652 fiber. Total dose: 65 kGy.

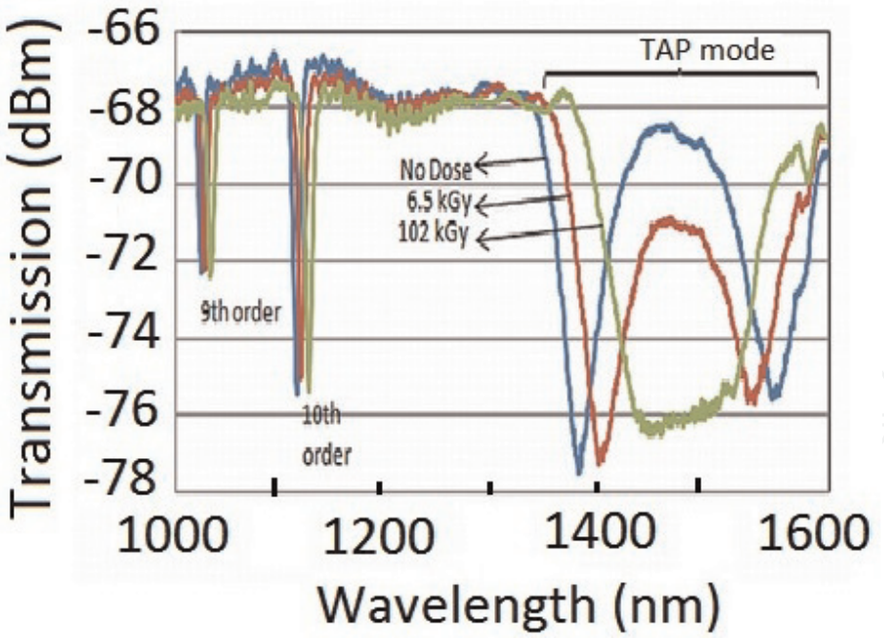

Figure 13.
Real-time resonance spectral measurements of TAP-LPG in gamma field [38].

The requirement of such sensors is divergent: for radiotherapy, we need very compact needle-like disposable tip sensors with very weak annealing properties. Once a patient is given a certain dose, the tip is discarded and a new dose sensing tip is used for other patients. For high dose sensing applications, the probe with high or low annealing may be desirable depending on application. For example, for long-term monitoring of integrated dose in waste storage facility will need very low annealing dose sensors while for repetitive dose measurements like gamma pencil fabrication, a high annealing rate sensor will be required.

6.6 Distributed gas sensors

The detection and identification of hazardous volatile compounds with low false alarm probability in large areas such as airports, underground metro stations, mines, bus stands, and major event arenas are a very daunting task. Other strategic applications include multi-point hydrogen leak detection systems for commercial and military launch vehicles that use cryogenic hydrogen as the main propellant. This gas is highly volatile, extremely flammable, and highly explosive. Hundreds of point gas sensors with electronic circuits are needed to cater big areas. Current detection systems use transfer tubes at a small number of locations through which gas samples are drawn and stream analyzed by a mass spectrometer. They are complex and costly systems and do not provide leak location.

Among several sensing systems, absorption-based systems are extensively explored and successfully employed. There have been serious efforts to develop absorption-based fiber optic systems for gas detection with higher sensitivity, fast response, and distributed sensing capability. They are based on measurement of VIS-IR-mid IR absorption by intended chemical species. The characteristic absorption spectra can be used as a fingerprint to identify a particular gas species. For example, many gas molecules have absorption lines in 0.8–1.8 μm band which is also a low loss transmission window of the silica fiber.

The spectral region of mid-IR is also a finger print region for most of the volatile compounds and nerve gases which is under investigation due to availability of compact tunable lasers in this band. The general principles of quantitative measurement of gas concentration have been described extensively in the literature [40, 41]. The basic principle is that the absorption is wavelength-dependent and compound specific. Initial systems used open path gas absorption cells comprising a pair of graded index collimator lenses with fiber pigtails [42]. The optical fibers here perform a passive role like transfer of light to and from absorption cell but play no active role in gas sensing. The National Aeronautics and Space Administration (NASA) reported a multi-point fiber optic multi-point hydrogen micro-sensor system for leak detection for launch vehicles [43]. The system consists of a multiplexed system having palladium coated micro lens attached to fiber tips. These chemically reactive coatings undergo changes in reflection in proportion to hydrogen concentration and are used as leak detectors. The invention of PCF or Holey fiber in 1990 opened new opportunities for exploiting the interaction of light with gases either through evanescent field or through hollow core region [44, 45]. The PCF family includes index guided PCF, hollow core photonic bandgap-fiber, and suspended core fiber.

6.6.1 Index guided photonic crystal fiber

Index-guided photonic crystal fibers are made with stack-and-draw process in fiber draw tower. They contain a periodic array of air holes running in cladding region and light is confined to solid core due to reduced effective index of the cladding. A fraction of evanescent field of power is extended into the holey region where it is absorbed by gas species and the gas concentration is obtained from intensity attenuation through the Beer-Lambert law. It is possible to design an IG-PCF that has a large fraction of evanescent power located within air-holes. This provides a good platform for gas sensing applications. Gas detectors based on absorption spectroscopy with IG-PCFs were experimentally demonstrated by Hoo et al. [46].

One concern in using IG-PCF as evanescent field sensors is the limited response time due to time required for sample gas to diffuse into holes from two open ends. Hoo et al. [46] have numerically calculated response time for acetylene gas in IG-PCF fiber (Λ = 1.55 μm, d = 1.4 μm) of length l with two ends open. When the fiber sensor length is 1 m, the time required to reach 90% concentration of exposed gas in surrounding is 200 min. This shows that we have to take a very short fiber if we require a response time of 1 min governed by diffusion time. However, this will reduce the sensitivity of the device due to limited path length. It is also observed that the relative sensitivity is also about 6% of that of open path cell per equal length. To achieve fast response time, one has to introduce periodic openings along the sensing fiber and measures like micro-pumping of sampling gases. To improve sensitivity, hollow core fibers may be a better choice as efficient interaction of guided light with gas molecules would be possible.

6.6.2 Hollow core photonic crystal fiber

Hollow core photonic crystal fiber is composed of a hollow core and a cladding with holes. The light is guided through the bandgap effect due to a proper design of hole sizes and gaps. They allow simultaneous confinement of optical mode and

gas phase materials within the hollow core. This provides an excellent means for strong light/molecular interaction inside the fiber core over long distance.

6.6.3 Enabling technologies

Critical issues related to distributed, high sensitivity, fast response sensors are mainly governed by the time required for gas to diffuse into the holes and open ends of the sensor fiber. One can introduce a number of transverse holes by using micro-structuring techniques. Various techniques for transverse micro-structuring have been reported. Hensley et al. [45] have reported gas cell fabrication using femtosecond micro-machining. Tightly focused laser pulses are used to produce micro-meter diameter radial channels in hollow core photonic crystal fiber, and through these micro-channels, the core of the fiber is filled with test gas. There are some reports about fabrication of microchannel by using 193 nm ArF laser. Viola et al. [43] have reported micro-hole drilling in hollow core mid-IR transmitting fibers by means of high power CO_2 laser shots.

6.6.4 Recent developments and existing fiber-based systems

Distributed gas sensors rely on depositing specific gas sensitive coatings as cladding in multi-mode fibers or gratings and OTDR method. Recently, many designs and configurations using PCFs have been reported which targeted better sensitivity and distributed detection capability. The advantage of waveguide-based sensors over open path multiple reflection cells included low gas volume, high photon to molecular interaction, and reduction of fringe effects. Whitenett et al. [47] reported the operation of a 64 point fiber optic methane sensor installed on a landfill site in Glasgow, UK. Though the environmental conditions are harsh, the sensor has performed satisfactorily, detecting methane in the range of ~50 ppm to 100% methane. Viola et al. [42] have reported development of a distributed nerve gas sensor based on mid-IR spectroscopy. This has been possible due to availability of tunable quantum cascade lasers in the 9–10 μm range, suitable hollow fibers for this band, and low noise cooled detectors.

7. Conclusion

India is poised to use nuclear power in a big way. The safety of these power stations will depend on monitoring the radiation levels near plant and at waste disposal sites. In such environments, conventional sensors have certain limitations. Fiber-based sensors are being developed all over the world and are expected to make significant contribution to safe operation of nuclear fuel cycle. New technologies of laser micro- and nano-processing, mid-IR transmitting fibers, and hollow fibers have opened development of new structures and devices like fast response PCF-based gas sensors, high temperature Bragg gratings, distributed nerve gas sensors, and distributed nuclear radiation sensors for home land security. On the other hand, availability of all silica nuclear resistant fibers and nano-fibers and possibility of grating writing in such fibers using focused ion beam source and femto-sec lasers have attracted their use for different parameter monitorings like structural health monitoring in nuclear reactors, tokamaks, and storage facilities.

Acknowledgements

The authors are thankful for the help received from Shri Jai Kishore, Smt. Smita Chaubey, and Shri Sanjai Kumar of Fiber Sensors Lab., RRCAT, Indore, in conducting various experiments.

List of acronyms

AS	anti-Stokes
CGCRI	Central Glass & Ceramic Research Institute
DE	dual-ended
DNA	deoxyribonucleic acid
DWT	discrete wavelet transform
EMI	electromagnetic interference
ESM-PCF	endless-single-mode photonic crystal fiber
FBG	fiber Bragg gratings
FIR	finite impulse response
IIR	infinite impulse response
ITER	International Thermonuclear Experimental Reactor
LHC	Large Hadron Collider
LPGs	long period gratings
MOSFET	metal-oxide semiconductor field-effect transistor
NASA	National Aeronautics and Space Administration
OSA	optical spectrum analyzer
OTDR	optical time domain reflectometry
PCFs	photonic crystal fibers
RGs	regenerated gratings
ROFDTSs	Raman optical fiber-based distributed temperature sensors
RRCAT	Raja Ramanna Centre for Advanced Technology
SNR	signal-to-noise ratio
St	Stokes
TAP	turn-around-point
TDM	time division multiplexing
TLD	thermoluminescent dosimeter
UV	ultraviolet
WDM	wavelength division multiplexing

Author details

Sanjay Kher* and Manoj Kumar Saxena
Fiber Sensors Lab., FSOSS, Raja Ramanna Centre for Advanced Technology, Indore, India

*Address all correspondence to: kher@rrcat.gov.in

IntechOpen

References

[1] Zhao XF, Li L, Ba Q, Ou JP. Scour monitoring system of subsea pipeline using distributed Brillouin optical sensors based on active thermometry. Optics and Laser Technology. 2012;**44**: 2125-2129

[2] Lopez RM, Spirina VV, Miridonova SV, Shlyagina MG, Beltran G, Kuzin EA. Fiber optic distributed sensor for hydrocarbon leak localization based on transmission/reflection measurement. Optics and Laser Technology. 2012;**34**: 465-469

[3] Culshaw B, Kersey A. Fiber-optic sensing: A historical perspective. Journal of Lightwave Technology. 2008;**26**: 1064-1078

[4] Grattan KTV, Sun T. Fiber optic sensor technology: An overview. Sensors and Actuators A Physical. 2000; **82**:40-61

[5] Dakin JP. Distributed optical fiber sensor systems. In: Culshaw B, Dakin J, editors. Optical Fiber Sensors: Systems and Applications. Vol. 2. Norwood, MA: Artech House; 1989. pp. 575-588

[6] Rogers AJ. Distributed optical-fiber sensors for the measurements of pressure, strain and temperature. Physics Reports. 1988;**169**:99-143

[7] Yilmaz G, Karlik SE. A distributed optical fiber sensor for temperature detection in power cables. Sensors and Actuators A Physical. 2006;**125**:148-155

[8] Hurtig E, Großwig S, Kühn K. Fiber optic temperature sensing: Application for subsurface and ground temperature measurements. Tectonophysics. 1996; **257**:101-109

[9] Höbel M, Ricka J, Wüthrich M, Binkert T. High-resolution distributed temperature sensing with the multiphoton-timing technique. Applied Optics. 1995;**34**(16):2955-2967

[10] Long DA. The Raman Effect. England: John Wiley; 2002. pp. 49-131

[11] Dakin JP, Pratt DJ, Bibby GW, Ross JN. Distributed optical fiber Raman temperature sensor using a semiconductor light source and detector. Electronics Letters. 1985; **21**(13):569-560

[12] Hill KO et al. Photosensitivity in optical fiber waveguides: Application to reflection fiber fabrication. Applied Physics Letters. 1978;**32**:647-649

[13] Kersey AD, Davis MA, Patrick HJ, LeBlanc M, Koo KP, Askins CG, et al. Fiber grating sensors. Journal of Lightwave Technology. 1997;**15**(8): 1442-1463

[14] Shimada Y, Nishimura A. Development of optical fiber Bragg grating sensors for structural health monitoring. Journal of Laser Micro/ Nano Engineering. 2013;**8**(1):110-114

[15] Kashyup R. Fiber Bragg Gratings. San Diego, CA, USA: Academic Press; 1999

[16] Kher S, Srikanth G, Chaube S, Chakraborty AL, Nathan TPS, Bhawalkar DD. Design, development and studies on Raman based fiber-optic distributed temperature sensor. Current Science. 2002;**83**(11):1365-1368

[17] Kher S, Srikanth G, Saxena MK, Nathan TPS. Development of distributed fiber optic temperature sensor with sub-meter resolution. Current Science. 2004;**86**(9):1202-1204

[18] Chakraborty AL, Sharma RK, Saxena MK, Kher S. Compensation for temperature dependence of Stokes signal and dynamic self-calibration of a

Raman distributed temperature sensor. Optics Communication. 2007;**274**: 396-402

[19] Chakraborty AL, Kher S, Chaubey S, Nathan TPS. Bidirectional frequency-domain digital filtering to simultaneously improve temperature resolution and eliminate spatial inaccuracy of a distributed temperature sensor. Optical Engineering. 2004; **43**(11):2724-2729

[20] Stoddart PR, Cadusch PJ, Pearce JB, Vukovic D, Nagrajah CR, Booth DJ. Fiber optic distributed temperature sensor with an integrated background correction function. Measurement Science and Technology. 2005;**16**(6): 1299-1304

[21] Saxena MK, Raju SDVSJ, Kher S, Arya R, Ravindranath SVG, Kher S, et al. Optical fiber distributed temperature sensor using short term Fourier transform based simplified signal processing of Raman signals. Measurement. 2014;**47**:345-355

[22] Guang-yong X, Jian-ping Y, Kun-jun Z, Wen M. Monitoring data processing of distributed optical fiber temperature sensor based on multi-wavelet. In: Proceedings of the International Workshop on Education Technology and Training & International Workshop on Geoscience and Remote Sensing. 2008. pp. 203-206

[23] Saxena MK, Raju SDVSJ, Arya R, Pachori RB, Ravindranath SVG, Kher S, et al. Raman optical fiber distributed temperature sensor using wavelet transform based simplified signal processing of Raman backscattered signals. Optics & Laser Technology. 2015;**65**:14-24

[24] www.google.co.in/search?q=BACKSCATTERED+LASER+LIGHT&source=lnms&tbm=isch&sa=X&ved=0ahUKEwiCvf-iq9jcAhWKT30KHdJ4CjYQ_AUICigB&biw=1093&bih=530

[25] Fukuzawa T, Shida H, Oishi K, Takeuchi N, Adachi S. Performance improvements in Raman distributed temperature sensor. Photonic Sensors. 2013;**3**(4):314-319

[26] Fernandez AF, Rodeghiero P, Brichard B, Berghmans F, Hartog AH, Hughes P, et al. Radiation-tolerant Raman distributed temperature monitoring system for large nuclear infrastructures. IEEE Transaction on Nuclear Science. 2005;**52**(6):2689-2694

[27] Lee CE. Self-calibrating technique enables long-distance temperature sensing. Laser Focus World. 2007;**43**: 101-117

[28] Suh K, Lee C. Auto-correction method for differential attenuation in a fiber-optic distributed-temperature sensor. Optics Letters. 2008;**33**(16): 1845-1847

[29] Zhang H, Wang Q, et al. Fiber Bragg grating sensor for strain sensing in low temperature superconducting magnet. IEEE Transactions on Applied Superconductivity. 2010;**20**(3): 1798-1801

[30] Marcelo M, Allil RCSB, de Nazar FVB. 14. Chapter "A Guide to Fiber Bragg Grating Sensors": In: Current Trends in Short- and Long-period Fiber Gratings. 2013

[31] Gusarov AI, Starodubov DS, et al. Comparative study of MGy dose level γ-radiation effect on FBGs written in different fibers. In: Proceedings of the OFS-13; April 12–16, 1999; Kyongju, Korea

[32] Gusarov AI, Chojetzkib C, et al. High total dose radiation effects on temperature sensing Fiber Bragg gratings. IEEE Photonics Technology Letters. 1999;**11**(9):1159-1961

[33] Krebber K et al. Fiber Bragg gratings as high dose radiation sensors.

Measurement Science & Technology. 2006;**17**:1095-1102

[34] Kher S, Chaube S, et al. Fiber optic temperature-insensitive, strain sensors for nuclear applications. International Journal of Applied Engineering and Technology. 2011;**1**(1):61-67. Available from: http://www.cibtech.org/J-ENGINEERING-TECHNOLOGY/PUBLICATIONS/2011/Vol%201%20No.%201/16-03-JET-Kher.pdf

[35] Henschel H et al. High radiation sensitivity of Chiral long period gratings. IEEE Transactions on Nuclear Science. 2010;**57**(5):2915-2922

[36] Rego G et al. Effect of ionizing radiation on the properties arc-induced long period fiber gratings. Applied Optics. 2005;**44**(29):6258-6263

[37] Gusarov AI et al. Comparative study of MGy dose level γ-radiation effect on FBGs written in different fibers. In: Proceedings of the OFS-13; April 12–16, 1999; Kyongju, Korea

[38] Kher S, Chaubey S, Kashyap R, Oak SM. Turnaround-point long period fiber gratings (TAP-LPGs) as high radiation dose sensors. IEEE Photonics Technology Letters. 2012;**24**(9):742-744

[39] Kher S, Chaubey S, Oak SM. Long period fiber grating based nuclear radiation sensors for high level dose applications. Journal of Instrumentation Science & Technology. 2013;**41**(2):135-142

[40] Bernath FP. Spectra of Atoms and Molecules. New York: Oxford University Press; 2005

[41] Svanburg S. Atomic and Molecular Spectroscopy: Basic Aspects & Practical Applications. Berlin: Springer; 2004

[42] Ho HL, Jim W, Demoken MS. Quantitative measurement of acetylene by using external cavity tunable diode laser. In: Proc. SPIE 3852, Harsh Environment Sensors II; Boston, US. 1999. pp. 124-133

[43] Viola R, Liberatore N, et al. Distributed nerve gases sensor based on IR absorption in hollow optical fiber. SPIE Proceedings. 2010;**7838**:78380H

[44] Kazemi AA, Goepp JW, et al. Fiber optic microsensro hydrogen leak detection system on aerospike X-33. In: SPIE Proceedings 6758, Photonics in the Transportation Industry: Auto to Aerospace; Oct. 2007

[45] Hensley CJ, Broaddus DH, et al. Photonic bandgap fiber gas cell fabricated using fs micromachining. Optics Express. 2007;**15**(11):6690-6695

[46] Hoo YL, Jin W, et al. Design and modeling of a photonic crystal fiber gas sensor. Applied Optics. 2003;**22**(18):3509-3515

[47] Whitenett G et al. Optical fibre instrumentation for environmental monitoring applications. IOP Journal of Optics A: Pure and Applied Optics. 2003;**5**:S140-S145